A Non Symmetric Interfacial Area Density Formulation for Transcritical CO2 Ejectors CFD Modeling

Egoi Ortego Sampedro

A Non Symmetric Interfacial Area Density Formulation for Transcritical CO2 Ejectors

Egoi ORTEGO SAMPEDRO

Mines ParisTech, Centre d'Efficacité Energétique des Systèmes, Palaiseau, France

egoi.ortego@mines-paristech.fr

ABSTRACT

The reduction of global warming potential gases emissions in industrial refrigeration devices requires the development of efficient cycles using low GWP gases. The supercritical $C0_2$ cycle assisted by a transcritical two phase ejector is a nice example of such cycles. The design of such ejectors is not obvious and an intense development of performance prediction tools is observed in literature especially regarding two-phase CFD modeling. The two phase flow CFD models are limited today by their lack of flexibility and difficulties to empirically calibrate them. The main drawback of classical Hertz-Knudsen or HRM phase change models is their difficulty to simultaneously predict the mass flow rate and the outlet velocity of the primary flow of the ejector. These two parameters are responsible of the entrainment ratio an ejector at given operating conditions and geometry. This paper presents a thermal phase change model that introduces a non symmetric interfacial area density formulation for two-phase liquid-gas CO_2 ejectors. This formulation describes the gas-liquid interface as bubbles at low void fractions and as droplets at high void fractions. The model results are compared to experimental results of literature. It appeared that bubbles number density affects mainly the primary flow rate and the droplets number density affects the outlet velocity of the primary nozzle and thus the mixture pressure and the secondary flow rate.

1. INTRODUCTION

The interest on natural refrigeration fluids is increasing due to the legal obligations on high GWP fluids for several countries. The CO_2 seems to be a good low GWP fluid candidate for different refrigeration uses. Throttling loses of refrigeration cycles is one of the major exergy production items (Elbel & Lawrence, 2016). It is particularly the case of transcritical CO2 cycles and great effort is done by several researchers to reduce those loses. For example the design of ejector assisted transcritical cycles is largely studied. The design process of such two-phase ejectors presents some difficulties in the prediction of several parameters such as the critical mass flow rate of the primary nozzle, the entrainment ratio and the critical pressure. Several authors worked on prediction methods of those parameters by 1D or more complex modeling; the most challenging aspect of simulations consists in the development of the right mass transfer modeling between the two cohabiting phases. The Homogeneous Relaxation Model (HRM) has been studied by different authors; it is based on the work of Downar-Zapolski et al. who proposed it initially for flashing flows in water nozzles (P.Downar-Zapolski, et al., 1996). The model is based on the actual and equilibrium vapor quality difference to compute the evaporation rate of the liquid. The empirical constants of this model were later adapted to the case of CO2 primary nozzles (Angielczyk, et al., 2010). That model was then used in a multitude of numerical studies that shown the ability of HRM to model the two-phase flow occurring in CO2 transcritical ejectors (Colarossi, et al., 2012), (Palacz, et al., 2017), (Michal, et al., 2018). One of the difficulties of that model is the calibration of empirical parameters it contains and that seems laborious to operate according to the calibration procedure proposed by Michal et al. (2018). Nevertheless a new set of empirical parameters was proposed depending on the motive nozzle inlet pressure; those parameters, when applied again to the cases, lead to reasonably good results on primary flow rate but produced errors always higher than 10% for the secondary flow rate. Other methods were tested to compute evaporation rate. For example formulations based on difference between liquid and saturation temperatures and a unique accommodation coefficient produced interesting results for CO2 transcritical nozzles pressure profile prediction (Giacomelli, et al., 2018); that paper introduces accommodation coefficients for evaporation and condensation as calibration parameters. More recently a model based on actual and inlet saturation pressure difference, similar to those used for standard cavitation problem (Singhal & Athavale, 2002), was tested for CO2 ejectors (Bodys, et al., 2020). The authors calibrated the accommodation coefficient of the mass transfer model and proposed a correlation to estimate it based on the inlet pressure and enthalpy of the motive nozzle. During the verification computational campaign, the primary mass flow rate could be relatively well predicted but the inaccuracy of the secondary mass flow rate was above 20% in the majority of cases.

The ability of the models mentioned before remains limited and for further research on phase change modeling seems necessary. In that perspective one can read the work done in the area of loss of coolant accidents (LOCA) water flash nozzles research. In that area, one of the main goals was to predict the critical mass flow rate in case of rapid loss of coolant in nuclear plants. A nice literature review was done by Yixiang et al. who made an overview of physical aspects of the phase change phenomena and modeling strategies for depressurizing flash flows (Yixiang & Dirk, 2017). The thermal phase change model (TPCm) discussed in that review appears to be

a good candidate for our purpose. It was successfully used for critical mass flow rate, pressure and void fraction profiles CFD computation by Yixiang et al. (Yixiang & Dirk, 2015) ; it was initially proposed by (B.J.C. Wu, 1981) for 1D modeling. This model computes the evaporation rate as a function of the liquid vapor interfacial heat transfer rate; the last depends on the actual liquid and saturation temperature difference, the interfacial heat transfer coefficient and the interfacial area density. In the present paper an adaptation of the TPCm for CO_2 transcritical ejectors is proposed and explored. That adaptation concerns the interfacial area density. It allows the TPCm being flexible and thus capable to model what happens at the motive nozzle's throat and outlet independently. That feature could make this model able to predict simultaneously the primary and the secondary mass flow rates of the ejector. The article presents first the general equations treated by the multiphase CFD solver. Then the non-symmetric thermal phase change model (nsTPCm) is presented. Subsequently test cases geometry and operating conditions are presented, followed by the simulation results and discussion.

2. Constitutive equations

2.1. Conservation equations formulation

The general formulation of conservation equations for a two phase flow requires a phase per phase description. In the commercial CFD code Ansys CFX 16.0 these equations, describing the so called Euler-Euler model, are described by equations (1) to (4) for liquid. The same kind of equations is used for liquid and gas; index 1 is used for the liquid and 2 for the gas.

Continuity equation:

$$\frac{\partial}{\partial t}(\alpha_1\rho_1) + \nabla\left(\alpha_1\rho_1\vec{U}_1\right) = \Gamma_{12} \tag{1}$$

where Γ_{12} is the volumetric mass flow rate transferred from liquid to vapor. And $\Gamma_{12} = -\Gamma_{21}$.

Momentum equation:

$$\frac{\partial}{\partial t}\left(\alpha_1\rho_1\vec{U}_1\right) + \nabla\left(\alpha_1\left(\rho_1\vec{U}_1\otimes\vec{U}_1\right)\right) = -\alpha_1\nabla p + \nabla\left(\alpha_1\mu_1\left(\nabla\vec{U}_1 + \left(\nabla\vec{U}_1\right)^T\right)\right) + \Gamma_{12}\vec{U}_i + \vec{M}_1 \tag{2}$$

The term $\Gamma_{12}\vec{U}_i$ is the momentum source produced by phase change. The term $\vec{M}_1$ contains the forces transferred from phase 2 to phase 1 i.e. the interfacial drag forces.

Total energy equation:

$$\frac{\partial}{\partial t}(\alpha_1\rho_1 h_1^t) - \alpha_1\frac{\partial P}{\partial t} + \nabla\left(\alpha_1\rho_1\vec{U}_1 h_1^t\right) = \nabla(\alpha_1\lambda_1\nabla T_1) + \alpha_1\nabla\left(\vec{U}_1\tau_1\right) + \Gamma_{12}h_i^t + \dot{q}_1 \tag{3}$$

where $\dot{q}_1$ is the interfacial heat transfer rate.

The interfacial transfer terms $\Gamma_{12}\vec{U}_i$ and $\Gamma_{12}\ h_i^t$ take into account the flux direction as follows:

$$\begin{matrix} if\ \Gamma_{12} < 0 \\ if\ \Gamma_{12} > 0 \end{matrix}\ \vec{U}_i = \begin{cases}\vec{U}_1 \\ \vec{U}_2\end{cases} and\ h_i^t = \begin{cases}h_1^t \\ h_2^t\end{cases} \tag{4}$$

The CFX solver solves also the volume continuity equation, or volume fraction transport equation, expression (5), usually introduced in multiphase problems. Thus, in the general case 6 (+1) equations are solved.

$$\sum_p \frac{1}{\rho_p}\left(\frac{\partial\left(\alpha_p\rho_p\right)}{\partial t} + \nabla\left(\alpha_p\rho_p\vec{U}_p\right)\right) = \sum_p \frac{\Gamma_{pp\prime}}{\rho_p} \tag{5}$$

The index p refers to the phase (1 or 2) and the index p' to the remaining phase (i.e. 2 or 1).

From that general formulation of conservation equations, some assumption can be done to simplify the problem. For the present work, the vapor was assumed to be saturated thus the energy equation wasn't resolved for vapor. That assumption is based on the works of P. Downar Zapolski et al. (1996) and Yixiang & Dirk (2015) of flash nozzles modeling.

2.2. Interfacial transfer terms

The mass transfer models are rather diverse. As it was written above the mass transfer can be modeled as being proportional to a quality, pressure or temperature difference between actual and saturated states. The proportionality factor depends on several aspects and the literature shows a great diversity of formulations. For this paper the so called thermal phase change model was used. The basic idea is to describe the mass transfer rate as a function of the heat flux associated with the phase change. The mass flux is:

$$\Gamma = \frac{\dot{q}_i}{\Delta h_{gl}^t} = \frac{h_i\, A_i}{\Delta h_{gl}^t(P)} \left(T_{sat}(P) - T_{liq}\right) \tag{6}$$

where h_i is the interfacial heat transfer coefficient, A_i is the interfacial area density (in $m^2/m3$) and Δh_{gl}^t is the total enthalpy difference between the gas and liquid. The interfacial heat flux ($\dot{q}_i$) is applied also to the energy balance. This expression shows the relation between the capacity of the fluid to internally transfer heat from liquid to vapor and its ability to phase changing.

Regarding the heat transfer coefficient, Yixiang (Yixiang & Dirk, 2015) proposed to use the Aleksandrov heat transfer coefficient that was derived from bubble growth analysis in superheated liquids (Avdeev, 2014) to take into account the gas/liquid velocity difference through the Péclet number.

$$h_c = \frac{\lambda_l}{l_c}\left(\frac{12}{\pi^2}\, Ja^2 + \frac{1}{3\pi} Pe\right)^{1/2} \tag{7}$$

where λ_L is the liquid's thermal conductivity and l_c is the interfacial characteristic length. The Jakob number is:

$$Ja = \frac{C_p \rho_l (T_l - T_{sat})}{\rho_g\, \Delta h_{gl}^t} \tag{8}$$

where C_p and ΔH_{gl} are respectively the isobaric heat capacity, and the latent heat of the liquid. The Péclet number is:

$$Pe = \frac{\left|\vec{U}_g - \vec{U}_l\right| l_c}{D_{T,l}} \tag{9}$$

where $D_{T,l}$ is the thermal diffusivity of liquid. In the cited Yixiang model, the heat transfer coefficient is multiplied by a correction factor k_h in order to add a calibration parameter to the formulation.

Regarding the formulation of the interfacial area density (A_i in equation (6)), some assumptions need to be done in order to avoid using detailed interface tracking techniques. A solution proposed by some authors is to model the transport and source terms of scalars associated with interfacial area. This is the case of the MUSIG (multiple size group) model that resolves the momentum equation for the dispersed phase using an Euler-Euler flow description (Eckhard Krepper, 2008). It is based on a bubble population balance equation. This model has evolved later to introduce the transition to the continuous gas phase (GENTOP model) in an attempt to obtain a general model (Susann Hänsch, 2012). The difficulty these methods try to address is the treatment of the diversity of characteristic sizes, and velocities describing a multiphase flow. It requires additional transport equations (one per sub-size fraction for inhomogeneous MUSIG model) and a variety of models for shape transition, coalescence or breakup source terms, etc. Nevertheless the generalization seems hard to achieve.

A simpler approach consists in proposing a relation between the void fraction and the interfacial area density. Wu (B.J.C. Wu, 1981) defines it for the first stage of phase change of flash flows as function of the void fraction and the number of bubbles per unit volume (N_b) Assuming equal sized spherical bubbles, Wu writes:

$$A_{i_b} = (6\alpha)^{2/3} (\pi\, N_b)^{1/3} \tag{10}$$

The value of the bubble number was assumed to be constant by Wu. When the void fraction increases, the bubbly flow should evolve to a bubbly-slug flow and then it should attain a mist flow regime. According to Wu, for the mist flow, the interfacial area density for constant sized droplets is:

$$A_{i_d} = (6(1-\alpha))^{2/3}(\pi\, N_d)^{1/3} \tag{11}$$

The number of droplets per unit volume (N_d) was assumed to be equal to N_b by Wu. Wu proposed a symmetric model assuming that transition from bubble to droplet regime is done at constant area density from 0.3 to 0.7 void fractions.

In the present work a non-symmetric bubble to droplet transition model was explored. To the knowledge of the author, this is the first time this is implemented in an ejector or in any flash flow situation. Equations (10) and (11) were maintained and a simple linear interpolation was implemented between $Ai_b|_{\alpha=0.3}$ and $Ai_d|_{\alpha=0.7}$.

In Ansys-CFX, for Euler-Euler problems composed of two continuous phases, the interfacial area density is expressed as follows:

$$A_i = \frac{\alpha(1-\alpha)}{l_c} \tag{12}$$

The interfacial length scale l_c has to be set by the user. That can be a constant or a variable. It was here defined by a CEL expression (in CFX, a kind of user defined function). In order to avoid getting non defined values of l_c at α values of 0 and 1, the volume fraction is capped to a certain minimum value; a value of 1e-7 was taken for this work. Note that liquid volume fraction is $(1-\alpha)$ and A_{i_b} and A_{i_d} are null at 0 and 1 void fractions respectively. Two examples of interfacial area densities are given by Figure 1 and Figure 2. The part of the curb starting at $\alpha = 0$ is A_{i_b} and the part at high values of α corresponds toA_{i_d}.

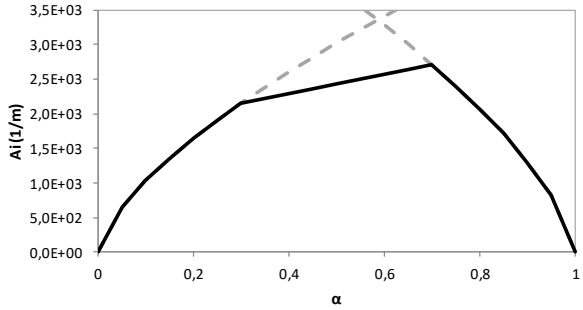

Figure 1 : non symmetric interfacial area density example $N_b = 1.10^9$ and $N_d = 2.10^9$

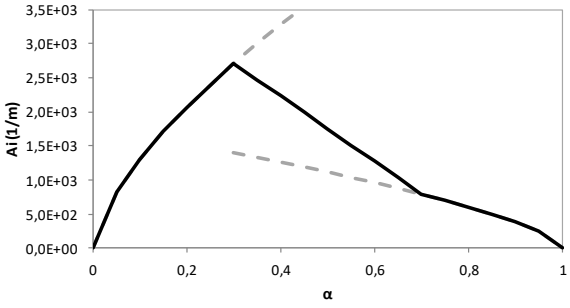

Figure 2 : non symmetric interfacial area density example $N_b = 2.10^9$ and $N_d = 5.10^7$

The interface momentum transfer term ($\vec{M}_{12}$ in equation 2), includes the drag force between liquid and gas. It has the following form (Ansys, 2014):

$$\overrightarrow{D_I} = \frac{C_D}{8} A_i\, \rho_l \left(\overrightarrow{U_2} - \overrightarrow{U_1}\right)\left|\overrightarrow{U_2} - \overrightarrow{U_1}\right| \tag{13}$$

No other interfacial forces were modeled here and thus $\vec{M}_{12} = \overrightarrow{D_I}$. Some tests on water flash nozzles were done by the author based on the formulation studied by Yixiang (Yixiang & Dirk, 2015). Drag force was modeled using Ishhii-Zuber, Schiller-Neumann (Ansys, 2014) and constant drag coefficient and no significant differences were found, notably, the Schiller-Neumann model computed a constant value of 0.44 in the entire diverging section of the nozzle. That's why a constant C_D value was used for the present work. That should be subject of further research since the interaction between liquid and vapor could be a parameter affecting the ejectors diffuser global behavior.

3. Test cases

One of the intentions of this paper is to discuss the advantages of modeling the transition from bubbles to droplets in the interfacial area density formulation. The bubble and droplet numbers may depend on several parameters, that's why test cases with different inlet/outlet conditions are interesting for the purpose of the article. Pazlack et al. (Palacz, et al., 2017) published an interesting set of data for transcritical CO_2 ejectors used for commercial refrigeration. The geometrical parameters were those corresponding to the ejector named EJ2 in the various papers of the same authors (Haida, et al., 2016)(Michal Haida, et al., 2019). The geometry of the retained ejector is presented in Figure 3.

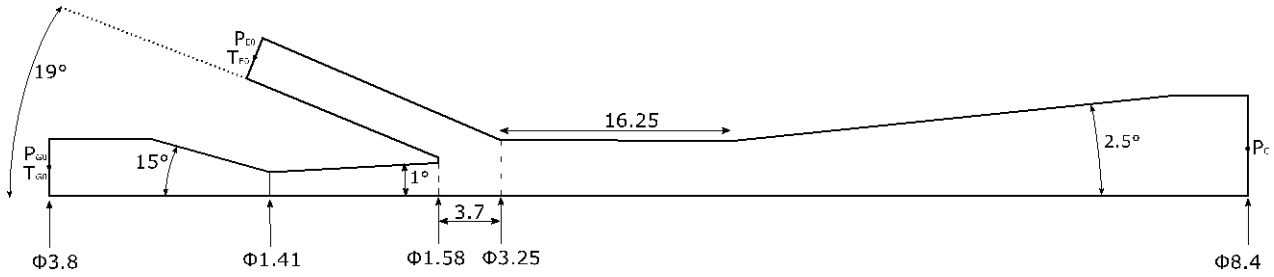

Figure 3 : EJ2 (Haida, et al., 2016) dimensions; lengths and diameters in mm and boundary conditions

The data used here are the ones reported in (Michal Haida, et al., 2019). The data set of EJ2 is presented in the **Table 1**.

Table 1 : set of operating points(Michal Haida, et al., 2019)

N°	$P_{G0}(bar)$	$T_{G0}(°C)$	$P_{E0}(bar)$	$T_{E0}(°C)$	$P_C(bar)$	$\dot{m}_G(kg/s)$	$\dot{m}_E(kg/s)$	μ
1	94,46	35,28	27,21	2,6	32,85	0,084	0,035	0,417
2	86,04	31,33	27,32	0,46	32,9	0,079	0,032	0,409
3	91,91	30,98	31,41	5,28	38,24	0,095	0,033	0,344
4	87,86	28,4	31,55	5,51	38,29	0,097	0,032	0,326
5	80,62	26,25	31,58	5,34	38,48	0,090	0,025	0,278
6	78,45	28,56	31,72	5,71	38,28	0,073	0,026	0,349
7	76,56	28,34	27,33	0,86	32,87	0,067	0,028	0,411
8	75,79	28,07	28,17	2,58	36,8	0,067	0,011	0,166
9	66,51	22,41	28,21	2,21	34,85	0,072	0,014	0,192
10	66,62	22,38	27,87	1,78	32,88	0,072	0,022	0,304
11	61,79	20,27	29,93	3,58	33,87	0,072	0,019	0,259
12	59,27	18,43	29,14	4,29	34,83	0,076	0,009	0,116
13	58,41	10	27,82	4,56	34,83	0,103	0,007	0,064
14	53,93	6,33	27,3	5,7	34,23	0,100	0,0031	0,031

4. CFD computations

In this section the configuration of the CFD solver, a summary of the physical formulation, a mesh sensitivity test and test results are presented.

4.1. Configuration and models

The ejector had as boundary conditions static pressures at primary inlet, secondary inlet and outlet, temperature at the primary inlet and liquid and vapor void fractions at the both inlets. The inlet liquid void fraction was set to 1 at the primary inlet and 0 at the secondary inlet. The wall was configured with default parameters of CFX. The nozzle flow was supposed to be axisymmetric. A 3° revolution form was therefore used to model the control volume with two symmetry planes as its limits.

The Peng –Robinson equation of state was used for liquid and vapor. For pressures below the critical pressure, vapor was considered to be saturated. Saturated state assumption was done because the vapor enthalpy varies modestly with the superheating degrees of the considered operating conditions and this has little effect on the theoretical entrainment ratio (around 3%); this value was computed with a 1D model based on the work of Chen et al. (Chen, et al., 2014) and adapted for 2 phase flows regarding the shock computation(Lee, et al., 2017). For pressures above the critical pressure, vapor's temperature was clipped at critical temperature. The liquid properties (ρ, C_p, μ) are function of the temperature computed from the enthalpy resulting from the energy balance. That means that when the flow gets into the two phase situation, the liquid's meta-stable condition is computed by considering it in a temperature based saturation state and not in a pressure based saturation state. The kwSST closure was used as turbulence model since this is the one preferred for adverse pressure gradient flows (Ansys, 2014). The CFX solver is a coupled solver using a pseudo-transient formulation; the coupled option was selected for volume fraction as well. A bounded second-order upwind scheme was selected for advection. A steady state simulation was done. The physical time step was set in a range between 1.10^{-4} s and

1.10^{-8}s depending on the mesh size and the model. This parameter acts like a relaxation coefficient. The simulation was supposed converged when the mass and energy imbalance was lower than 0.5%, the inlet and outlet mass flow rates were stabilized; all residuals were in this situation lower than 1.10^{-5}. The flow field was initialized at 0 vapor volume fraction, at primary inlet temperature and pressure and at 0m/s velocity.

4.2. Mesh sensitivity

A mesh sensitivity analysis was conducted in order to choose a size leading to a reasonable precision within a reasonable computational time. The mesh was composed by prisms at the symmetry axis and hexahedrons everywhere else. The tested case is the N°7 and four meshes were evaluated. The results were monitored in terms of primary and secondary mass flow rates. The effect of mesh was quantified comparing the results to those of the more dense mesh. Table 2 gives the differences to the last case and the number of elements for each mesh tested.

Table 2 : mass flow rate variations

Number of nodes	8E+03	3,4E+04	5,7E+04	8,2E+04	1,4E+05
$\partial \dot{m}_G$	3,7%	1,2%	0,8%	0,3%	0,0%
$\partial \dot{m}_E$	11,6%	1,8%	1,5%	0,2%	0,0%

The retained mesh is the 3rd one for the rest of the computations.

4.3. Test cases

In this section the methods by which the models were calibrated are presented followed by the comparisons to the experimental results. For the models' accuracy comparison, a mean error is given for the available variables (φ); it is computed as follows:

$$er_{\varphi} = \frac{\varphi_{CFD} - \varphi_{REF}}{\varphi_{REF}} \tag{14}$$

One of the objectives of this work was to explore the ability of the described formulation to calibrate the results to the experimental data; that means being able to get the correct motive and secondary mass flow rates simultaneously. The hypothesis advanced when this work began was that the critical mass flow rate at the primary depends on the early phase change regime close to the nozzle throat and that the nozzle outlet velocity is strongly affected by the ending phase change regime close to the outlet. Then, since the velocity attained by the primary flow could strongly affect the secondary mass flow rate, the end of the phase change regime was supposed to affect the entrainment ratio.

The evolution of the phase change regime is well represented by the evolution of the interfacial area density since it models the constraints on transfer area at the start and the end points of the liquid-bubbles-droplets transition. The first calibrated parameter was the number of bubbles density in order to get the correct primary mass flow rate. Then the possibility of getting the secondary mass flow rate was explored by adapting the number of droplets density.

Some examples of the results obtained by the calibration procedure are represented in Figure 4; it plots the values of the simulated secondary and primary mass flow rates at different calibration steps. Each grey point represents a converged simulation result for a set of calibration parameters. The large points represent the reference values. The calibration was stopped when the discrepancies were close to 1% or when the variation of calibration parameter had no more effect on the results. The ability of the model to "move" on this solutions space attests to the flexibility of the model. Thanks to the combined adaptation of the Nb and Nd values it was possible to attain the target flow rates values for a majority of cases. Nb acts mainly on the primary flow rate and Nd on the secondary flow rate. An increase of Nb produces a reduction of the flow rate; this is related to a lower superheating degree needed for the evaporation to occur. That makes the cavitation inception pressure increase and makes cavitation start at lower throat flow velocities. An increase of Nd produces an increase of the secondary flow rate due to the primary flow velocity increase close to primary nozzle outlet.

For some cases the secondary flow rate target couldn't be obtained; the flow rate seams to attain a maximum or a minimum value despite the increase or decrease of Nd. That could be related to the use of a simplified EOS or to the errors introduced by the assumption of saturated state of vapor phase.

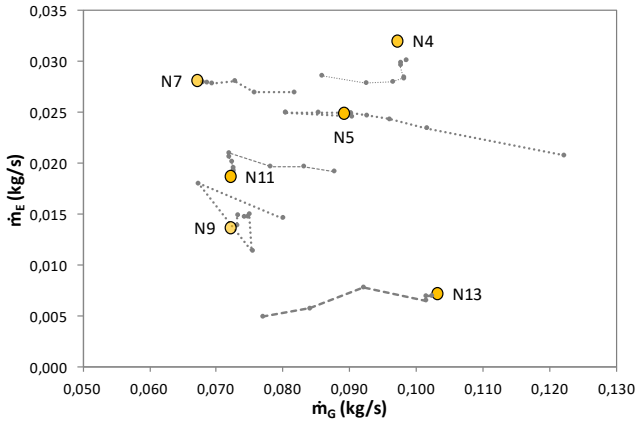

Figure 4 : mass flow rates: measured and during calibration

The list of the results is given in Table 3. That table gives also the values of the parameters at the last stage of calibration.

Table 3 : summary of errors and calibration parameters

Case N°	1	2	3	4	5	6	7	8	9	10	11	12	13	14
$er_{\dot{m}_G}$	1%	1,3%	1%	1,4%	1,4%	0,4%	1,3%	1%	1,4%	0,8%	0,9%	1,4%	0,7%	-1,2%
$er_{\dot{m}_E}$	**-32%**	**-22%**	**-15%**	-5,9%	-0,6%	0,9%	-0,6%	**10%**	1,6%	-2,5%	1,3%	0,9%	-0,6%	3,0%
N_b	2,5E+14	1,5E+15	7,0E+14	3,7E+14	8,0E+14	3,0E+15	3,7E+15	6,0E+15	2,2E+15	2,2E+15	1,7E+15	8,0E+14	1,8E+14	1,8E+14
N_d	3,0E+15	5,0E+15	4,0E+15	1,0E+16	4,0E+13	3,3E+13	4,0E+14	7,0E+11	5,0E+13	2,0E+15	1,0E+12	8,0E+11	3,6E+14	9,0E+10

The motive flow rate could be calibrated in a range of ±1.5% error for all cases. The entrained flow rate could be calibrated in a similar range of error for most cases but the first three cases and the N°8 present important errors; the first ones were obtained for motive inlet temperatures equal or above the critical temperature. The reason for this behavior is not yet clear but probably the modeling of the vapor phase needs to be improved since when the primary inlet temperature is super-critical, the saturated vapor conditions is clearly questionable in the flash region and vapor metastability should be considered.

Figure 5 shows liquid and saturation temperatures profiles on the center line of the ejector for cases N°13 and N°7. One can observe the apparent sub-cooling degree at the inlet for case N°13; it reduces suddenly close to the primary throat location. The pressure drop makes the liquid move towards a metastable superheated state.

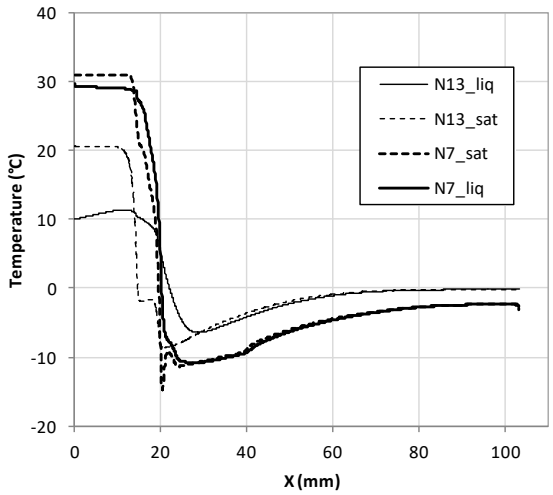

Figure 5 : liquid and saturation temperature profiles for cases N°13 and N°7

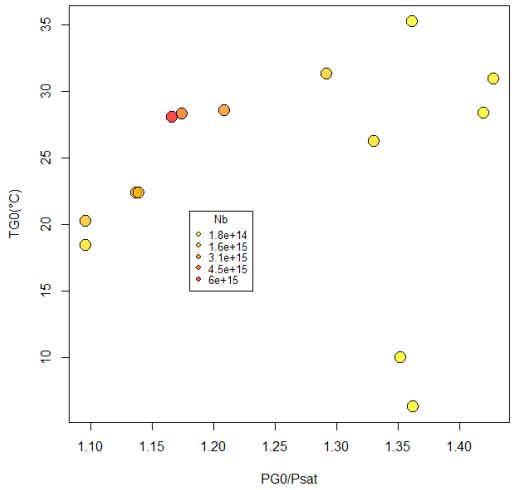

Figure 6 : values of Nb function of TE0 and PG0/Psat

This state is maintained up to the x=30mm location; after that point the liquid gets into an apparent sub-cooled state again. This is due to the compression in the end of the mixing chamber and in the divergent; the liquid temperature increases slower than the one of vapor. In this part of the ejector vapor is condensing.

Regarding the values of Nb and Nd, a way of predicting them is needed to generalize the model. The cavitation inception at the throat of flash nozzles has been largely studied (Yixiang & Dirk, 2017); it is frequently related to parameters such as the nucleation frequency, nucleation site density or number of bubbles density. Those parameters are often expressed as functions of initial or inlet temperature, pressure difference to saturation at the inlet or other parameters.

The prediction of Nb will not be treated here; nevertheless a plot showing the effect on Nb of T_{GO} and the ratio of P_{G0} to the isentropic saturation pressure is given in Figure 6. The isentropic saturation pressure is the pressure at which the inlet entropy line crosses the saturation curve. The value of Nb decreases with increasing pressure ratio and low inlet temperatures; it seems to increase at high temperatures and low pressure ratios.

Regarding the values of Nd, it should depend on the breakup regime and thus local Weber and Ohnesorge numbers. That could be also related to the Nb value since the number of liquid ligaments created during the transition from bubbles to droplets could depend on the initial bubbles number. Further research needs to be done in this direction in order to outline the variables affecting Nd.

5. Conclusion

This paper deals with CFD modeling of two phase flows in a CO_2 two-phase ejector. The paper explored the ability of a non symmetric thermal phase change model (nsTPCm) to predict the motive and suction mass flow rates. The particular formulation of the interfacial area density allowed the independent calibration of the both flow rates thanks to two adaptation parameters: the number of bubbles density was mainly affecting the motive flow and the number of droplets density the suction flow. The model is easy to calibrate and provides the minimum and sufficient number of degrees of freedom for two phase ejectors modeling.

The model seems to represent the flow correctly in sub-critical motive inlet temperature situations, even for supercritical pressures, but gives unsatisfactory results at super-critical temperatures. This preliminary work needs to be continued in order to provide a general formulation of the mass transfer phenomena in such expansion-entrainment flow situations. The first step should be using a real equation of state for the CO_2 and the behavior of the model at high temperatures needs to be investigated more in detail. Furthermore, a larger number of experimental data should be used in order to test the model. Also, further research needs to be done regarding the prediction of Nb and especially Nd parameters in order to develop associated nucleation and atomization sub-models.

NOMENCLATURE

Roman characters

A	interfacial area density [m^{-1}]
C_D	drag coeffiicient
C_P	isobaric heat capacity [J kg^{-1} K-
D_I	drag force[N m^{-3}]
D_T	thermal diffusivity [m^2 s^{-1}]
h^t	total enthalpy [J kg^{-1}]
h_i	interfacial heat transfer coefficie
Ja	Jakob number
K	relaxation coefficient
l_c	interfacial length scale [m]
N	number density [m^{-3}]
M	interface forces [N m^{-3}]
P	pressure [Pa]
P_e	Peclet number
P_r	Prandtl number
$\dot{q}_1$	interfacial heat transfer [W m^{-3}
R_g	universal gas constant [kg kmol
s	entropy [J kg^{-1} K^{-1}]
T	temperature [K]
U	velocity [m s^{-1}]
vof	volume fraction
x	quality

Greek characters

α	volume fraction
Γ	volumetric mass flow rate [$kg\ n$
η	isentropic efficiency
θ	relaxation time [s]
λ	thermal conductivity [W m^{-1}]
μ	dynamic viscosity [Pa s]
ρ	density [kg m^{-3}]
τ	viscous stresses
ϕ	mass transfer potential

Subscripts

0	Inlet
1	Liquid phase
2	Gas phase
G	Primary or motive
E	Secondary or suction
b	bubble
d	droplet
gl	gas to liquid
i	interfacial
in	inlet
out	outlet
s	isentropic
sat	saturated
p	first phase
p'	second phase

6. References

Abuaf, N., 1981. *A study of Nonequilibrium Flashing of Water in a Converging-Diverging Nozzle: Volume1. Experimental. U.S. Nuclear Regulatory Comission,* s.l.: s.n.

Angielczyk, W., Bartosiewicz, Y., Butrymowicz, D. & Seynhaeve, J.-M., 2010. *1-D Modeling Of Supersonic Carbon Dioxide Two-Phase Flow Through Ejector Motive Nozzle.* Purdue, s.n.

Ansys, 2014. *Ansys V16 Users Guide.* s.l.:s.n.

Avdeev, A. A., 2014. Laws of Vapor Bubble Growth in the Superheated Liquid Volume (Thermal Growth Scheme). *High Temperature,* 52(4), pp. 588-602.

B.J.C. Wu, N. A., 1981. *A study of Nonequilibrium Flashing of Water in a Converging-Diverging Nozzle: Volume2. Modelling. U.S. Nuclear Regulatory Comission,* s.l.: s.n.

Banasiak, K. et al., 2015. Development and performance mapping of a multi-ejector expansion work recovery pack for R744 vapour compression units. *International Journal of Refrigeration,* Volume 57, pp. 265-276.

Bodys, J., Smolka, J., Palacz, M. & Haida, M., 2020. Non-equilibrium approach for the simulation of CO2 expansion in two-phase ejector driven by subcritical motive pressure.

Bussac, F., 1985. *Developpement d'une turbine diphasique pour la production d'électricité à partir de la détente de saumures géomethermales,* s.l.: Commission des Communautés européennes.

Chen, J., Havtun, H. & Palm, B., 2014. Investigation of ejectors in refrigeration system: Optimum performance evaluation and ejector area ratios perspectives. *Applied Thermal Engineering,* pp. 182-191.

Colarossi, M., Trask, N., Schmidt, D. P. & Bergander, M. J., 2012. Multidimensional modeling of condensing two-phase ejector flow. *International Journal of Refrigeration,* pp. 290-299.

Eckhard Krepper, D. L. T. F. H.-M. P. P. J. Z., 2008. The inhomogeneous MUSIG model for the simulation of polydispersed flows. *Nuclear Engineering and Design,* Issue 238, pp. 1690-1702.

Elbel, S. & Lawrence, N., 2016. Review of recent developments in advanced ejector technology. *International Journal of Refrigeration,* Volume 62, pp. 1-18.

G.Eliot, D., 1982. *Theory and Tests of Two-Phase Turbines.* Pasadena: Jet Propulsion Laboratory.

Geng, L., Liu, H. & Wei, X., 2019. CFD analysis of the flashing flow characteristics of subcritical refrigerant R134a through converging-diverging nozzles. *International Journal of Thermal Sciences,* pp. 438-445.

Giacomelli, F., Mazzelli, F. & Milazzo, A., 2018. A novel CFD approach for the computation of R744 flashing nozzles in compressible and metastable conditions. *Energy,* Volume 162, pp. 1092-1105.

Haida, M. et al., 2016. Numerical investigation of an R744 liquid ejector for supermarket refrigeration systems. *Thermal Science,* 20(4), pp. 1259-1269.

H, S., 2006. *Gasdynamic Aspects of Two-Phase Flow.* Weinheim: Wiley VCH.

Jiro Sende, Y. H. H. F., 1994. Modeling on atomization and vaporization process in flash boiling spray. *JSAE Review,* Volume 15, pp. 291-296.

Karathanassis, I., 2017. Comparative evaluation of phase change mechanisms for prediction of flashing flows. *International Journal of Multiphase Flows,* Volume 97, pp. 257-270.

Lee, J., Lee, C., Baek, S. & Jeong, S., 2017. Investigation of ejector-equipped Joule–Thomson refrigerator operating below 77 K. *International Journal of Refrigeration,* Volume 78, pp. 87-107.

Le, Q. D., 2017. *FLASHING FLOW MODEL FOR INDUSTRIAL ENERGY APPLICATIONS.* s.l.:POLITECNICO DI MILANO.

Lorenzo, M. D. et al., 2017. Homogeneous two-phase flow models and accurate steam-water table look-up method for fast transient simulations. *International Journal of Multiphase Flow,* pp. 199-219.

Michal Haida, R. F. W. S. et al., 2019. An Object-Oriented R744 Two-Phase Ejector Reduced-Order Model for Dynamic Simulations. *Energies,* Volume 12.

Michal, H. et al., 2018. Modified homogeneous relaxation model for the R744 trans-critical flow in a two-phase ejector. *International Journal of Refrigeration,* pp. 314-333.

Ohta, J., 1993. Performance and flow characteristics of nozzles for initially subcooled hot water (influence of turbulence and decompression rate). *International Journal of Multiphasse Flow,* 19(1), pp. 125-136.

P.Downar-Zapolski, Z.Bilicki, L.Bolle & J.Franco, 1996. The non-equilibrium relaxation model for one-dimensional flashing liquid flow. *International Journal of Multiphase Flow,* Volume 22, pp. 473-483.

Palacz, M. et al., 2017. HEM and HRM accuracy comparison for the simulation of CO2 expansion in two-phase ejectors for supermarket refrigeration systems. *Applied Thermal Engineering,* Issue 115, pp. 160-169.

Palau-Salvador, G., Gonzalez-Altozano, P. & Arviza-Valverde, J., 2007. Numerical modeling of cavitating flows for simple geometries. *Spanish Journal of Agricultural Research.*

Reocreux, M., 1974. *Contribution à l'étude des débits critiques en écoulement diphasique eau-vapeur.* Grenoble: Université Scientifique et Médicale de Grenoble.

S. Maksic, D. M., 2002. CFD-CALCULATION OF THE FLASHING FLOW IN PIPES AND NOZZLES. *Proceedings of ASME FEDSM'02.*

Sara Vahaji, A. A., 2015. Study on the Efficiency of a Convergent-Divergent Two-Phase Nozzle as a Motive Force for Power Generation from Low Temperature Geothermal Resources. *Proceedings World Geothermal Congress.*

Singhal, A. & Athavale, M., 2002. Mathematical bases and validation of the full cavitation model. *J Fluids Eng,* Volume 124, pp. 617-624.

Susann Hänsch, D. L. E. K. T. H., 2012. A multi-field two-fluid concept for transitions between different scales of interfacial structures. *International Journal of Multiphase Flow,* Volume 47, pp. 171-182.

Yazdani, M., 2014. Numerical Modeling and Validation so Supersonic Two-Phase Flow of CO2 in Converging-Diverging Nozzles. *Journal of Fluid Engineering,* Volume 136.

Yixiang, L. & Dirk, L., 2015. 3D CFD simulation of flashing flows in a converging-diverging nozzle. *Nuclear Engineering Design,* pp. 149-163.

Yixiang, L. & Dirk, L., 2017. Computational modelling of flash boiling flows, a literature survey. *International Journal of Heat and Mass Transfer,* pp. 246-265.